Isr. J. Earth Sci.; 50: 9–22

Crustal deformation during 6 years spanning the M_w = 7.2 1995 Nuweiba earthquake, analyzed by Interferometric Synthetic Aperture Radar

Gidon Baer,[a] Gadi Shamir,[b] David Sandwell,[c] and Yehuda Bock[c]
[a]Geological Survey of Israel, 30 Malkhe Yisrael Street, Jerusalem 95501, Israel
[b]The Geophysical Institute of Israel, P.O. Box 182, Lod 71100, Israel
[c]Cecil H. and Ida M. Green Institute of Geophysics and Planetary Physics, Scripps Institution of Oceanography, La Jolla, California 92093, USA

(Received 15 March 2001; accepted in revised form 31 May 2001)

ABSTRACT

Baer, G., Shamir, G., Sandwell, D., Bock, Y. 2001. Crustal deformation during 6 years spanning the M_w = 7.2 1995 Nuweiba earthquake, analyzed by Interferometric Synthetic Aperture Radar. Isr. J. Earth Sci. 50: 9–22.

The November 22, 1995, M_w = 7.2 Nuweiba earthquake occurred along one of the left-stepping segments of the Dead Sea Transform in the Gulf of Elat (Aqaba). We examine the surface deformation patterns in the region by Interferometric Synthetic Aperture Radar (InSAR) for the period 1993 to 1999, which includes the end of one seismic cycle and the beginning of the next. Because the main rupture was under water, ERS coverage is limited to distances of approximately 5 km or more away from the rupture. Pre-earthquake interferograms do not show any detectable deformation along the Gulf. Coseismic interferograms show deformation at distances of up to 50 km from the main rupture, with the highest fringe rate (strain) NW of the rupture termination. Coseismic phase gradient maps show triggered slip along faults parallel to the main rupture (sinistral or normal with the Gulf side down) along the western shore of the Gulf, and in a belt of extensional faults along the eastern shore, striking at angles of about 30° to the major rupture. Postseismic deformation is observed only in a time window of up to 6 months following the mainshock. It was concentrated in the region of the high coseismic strain, and seems to be related to the $M_L > 4.5$ aftershocks in the respective time window.

INTRODUCTION

The temporally and spatially varying behavior of earthquakes in the Earth's crust has been recognized for almost a century (e.g., Gilbert, 1909; Reid, 1910), yet the mechanisms by which the Earth deforms throughout an earthquake cycle are still inadequately understood. The cycle of large earthquakes is often divided into four phases: preseismic, coseismic, postseismic, and interseismic. Geodetic observations from various locations have detected surface displacements associated with each of these phases. Quantifying the temporal deformation patterns is of great importance, because they reflect the way strain accumulates and is released, and have implications for the mechanism of strain accumulation, earthquake recurrence times, and crustal rheology.

In this respect a great step has been made in the last

E-mail: baer@mail.gsi.gov.il

 0021-2164/01 $4.00

two decades, with the introduction of two precise space-based geodetic techniques: Global Positioning System (GPS), and Interferometric Synthetic Aperture Radar (InSAR). These techniques, which provide displacement measurements at sub-centimeter accuracy, enable the determination of deformation rates and patterns over broader areas, and over considerably shorter time intervals than previously possible. InSAR has been shown to be particularly effective for mapping the displacement fields associated with earthquakes (e.g., Massonnet and Feigl, 1998, and references therein). As deformation rates are higher (and thus more readily measurable) in the coseismic and postseismic phases of the earthquake cycle, a large number of recent geodetic studies have focused on these two phases.

Continuous and periodic GPS measurements in the 3.5 years following the 1992 Landers earthquake in southern California suggest that postseismic strain released 10% to 20% of the seismic moment of the mainshock (e.g., Shen et al., 1994). The temporal behavior of this strain relaxation and its mechanism are still poorly understood, but it has been generally described as a short-term exponential relaxation superimposed upon a long-term linear trend. One way of identifying the strain release mechanism is by observing the rate of decay and the spatial extent of deformation following an earthquake. A larger extent of deformation with slower decay rates is generally attributed to viscoelastic relaxation or slip on the downward extension of the rupture (e.g., Thatcher, 1983), whereas small-scale relaxation patterns may be attributed to shallower processes closer to the fault zone, possibly related to fluid flow.

The November 22, 1995 M_w = 7.2 Nuweiba earthquake occurred along one of the left-stepping segments of the Dead Sea Transform (DST) in the Gulf of Elat (Fig. 1). It was the largest earthquake along the DST in the last few centuries (e.g., Ambraseys and Melville, 1989). The earthquake was preceded by earthquake swarms near both its rupture ends (Shamir, 1997). The mainshock was followed by intense aftershock activity, including nearly 200 events of $M_L \geq 4$ in the year following the mainshock (Hofstetter et al., 1998). The epicenter of the Nuweiba earthquake was at 28.76°N, 34.66°E, with an estimated nucleation depth of about 12.5 km. The earthquake initiated with a small sub-event which had a pronounced normal component, while the overall rupture was dominantly left lateral strike slip (Kikuchi, 1995; Shamir, 1996; Pinar and Turkelli, 1997; Hofstetter et al., 1998).

In a previous study (Baer et al., 1999) we analyzed the coseismic deformation of the earthquake using InSAR. In this study, we present improved InSAR results of the coseismic deformation due to extended data in the near range of the radar and a better digital elevation model (DEM). We extend the analyzed period to six years (1993–1999), spanning the end of one seismic cycle and the beginning of the next.

INTERFEROMETRIC SYNTHETIC APERTURE RADAR (INSAR)

Method

Interferometric analysis of SAR images has become a widespread, effective technique to measure subtle displacements at the ground surface (Gabriel et al., 1989; Massonnet and Feigl, 1998, and references therein). When two radar scans are made at different times from the same viewing angle, a small change in the position of the target (ground surface) may create a detectable change in the phase of reflected signals. This phase change is proportional to the path difference between the two signals, and thus may be translated to displacement along the satellite-to-ground line of sight. A component of this phase change is always generated by the topography in the target area; the topographic effect increases with the growing separation (baseline) between the two viewing antennae. To isolate the phase change caused by ground displacements from the topographic phase, the latter is removed. A low-resolution digital elevation model (DEM) is projected into the radar coordinates and removed from the full resolution interferogram. In addition to removing the crude DEM, the residual phase from a suitable Tandem ERS-1 to ERS-2 pair is unwrapped and added to the crude topographic phase model to form a full resolution topography model needed for isolating the phase signal due to ground motion. This hybrid approach of topographic phase construction retains the long-wavelength accuracy of the two-pass method (Massonnet and Feigl, 1998) and the full topographic resolution of the 4-pass method (Zebker et al., 1994).

The resulting (change) interferogram reflects the range changes primarily due to ground displacement, but also includes some artifacts due to orbital or signal propagation (atmospheric) errors and temporal and/or spatial decorrelation of the land surface. Repeat orbits are usually not parallel, necessitating the computation of a new baseline at every point in both azimuth and range within an image frame (e.g., Gabriel and Goldstein, 1988). In contrast to previous studies, which estimated baseline parameters from imagery,

topography data, and perhaps known ground control points, we compute baselines from ERS-1/2 precise orbits provided by Scharroo and Visser (1997). These orbits have radial accuracy of 50 mm and cross-over repeatability within 70 mm, giving an overall baseline accuracy better than 70 mm. The advantage of this approach is that surface displacements and long-wavelength atmospheric artifacts are not absorbed into the baseline estimate.

Methods of filtering interferograms range from simple averaging over pixels (taking looks) (e.g., Gabriel et al., 1989), to spatially variable filters whose power spectra are matched to that of the local phase (Goldstein et al., 1988; Werner et al., 1992). We filtered the real and imaginary parts of the complex interferogram (with pixel spacing as sampled by the radar) separately, using a low-pass Gaussian 5 point by 17 point filter that has a 0.5 gain at a wavelength of 200 m (Sandwell and Price, 1998).

Because we cannot yet remove the atmospheric signal from the topographic phase-corrected interferograms, it is important to be able to recognize atmospheric artifacts so they are not confused with deformation. Short-wavelength atmospheric artifacts (which could be confused with small-scale tectonic deformations) typically have length scales on the order of 5–10 km and can cause as much as 6 cm of excess two-way path length (2 interferogram fringes). Examples can be found in Massonnet and Feigl (1995), Rosen et al. (1996), Zebker et al. (1997), and Hanssen (2001). Interferograms showing obvious atmospheric contamination are discarded. Regional atmospheric effects corresponding to long-wavelength, ionospheric perturbations, and differences in the hydrostatic component of the troposphere manifest themselves as a planar phase trend in an interferogram (Tarayre and Massonnet, 1996). This phase trend makes it necessary either to compute an "artificial baseline" (Tarayre and Massonnet, 1996) or to remove the long-wavelength atmospheric effect from the interferogram at some point in the data processing. If these regional effects are not removed, they could be interpreted as a regional tilt. Each fringe cycle in the topography- and orbital-corrected change interferogram corresponds to contours of 28-mm ground displacement along the satellite-to-ground line of sight.

DATA

SAR data for this study were collected by the European Space Agency Remote Sensing Satellites ERS-1, which imaged the area between April 1992 and October 1997, and ERS-2, which has been imaging the area since July 1995. The SAR operates in C-band at a wavelength of 56.5 mm, with a nominal orbital cycle of 35 days for each satellite. During the overlapping period of the two satellites (1995–1997), they performed tandem missions at one-day intervals. For this

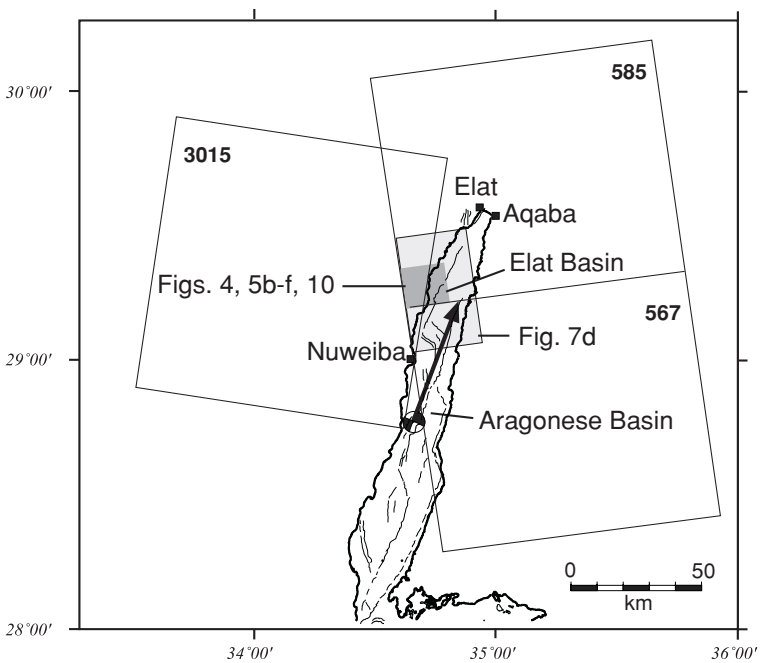

Fig. 1. Location map of the Gulf of Elat (Aqaba), showing the major faults, and the epicenter and general rupture trace of the Nuweiba earthquake (marked by arrow). Also shown are the SAR frames selected for interferometric analysis, and locations of Figs. 4,5,7, and 10.

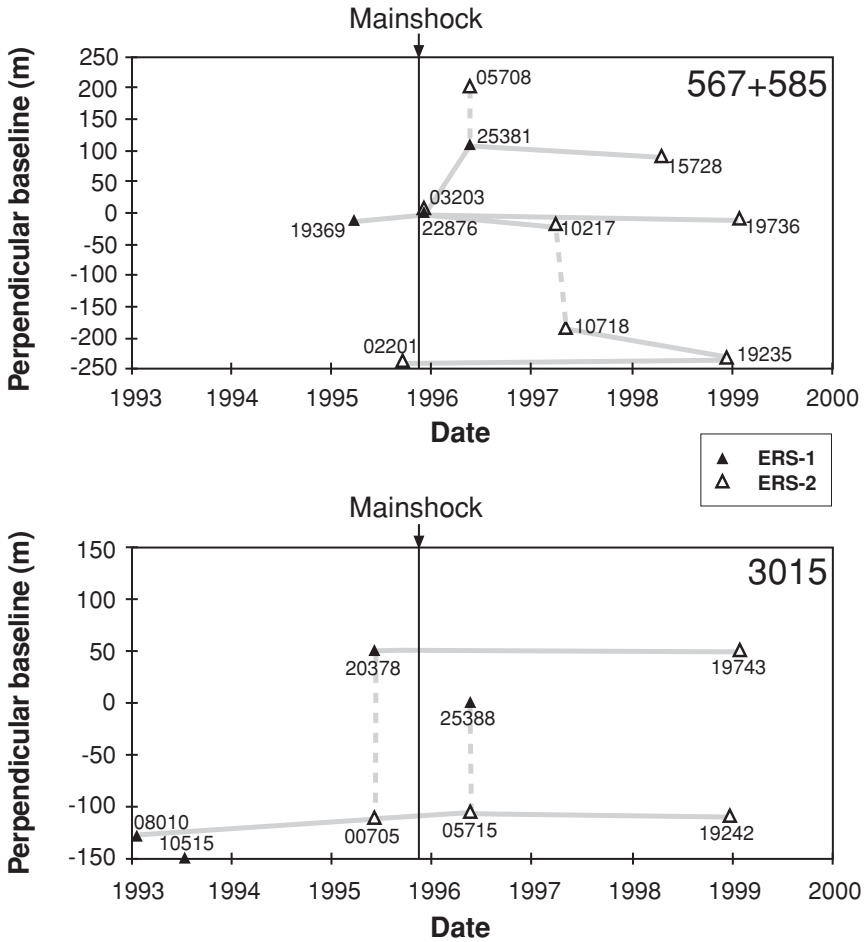

Fig. 2. Acquisition times and perpendicular baselines of orbits checked for this study. Grey solid and dashed lines represent pairs used for change and topographic interferograms, respectively. *Top*, frames 567 and 585, *bottom*, frame 3015.

study, we selected three 100 × 100 km SAR frames (Figs. 1,2): frames 567 and 585 (ascending track), and frame 3015 (descending track). Change (deformation) interferograms were generated for different time intervals of 3 to 71 months between 1993 and 1999 (Fig. 2). Only the descending track (frame 3015) has suitable data for interferometric analysis of the 3 pre-earthquake years (Fig. 2).

RESULTS

Coseismic and postseismic interferograms

We have generated a new interferogram in the two eastern (ascending track) frames for the period 21/9/95–24/12/98 (Fig. 3). The interferogram shows 3 zones of pronounced (coseismic + postseismic) displacements, one on the western side of the Gulf, with a maximum satellite-to-ground range change of about 15 cm, and two zones on the eastern side of the Gulf, with range changes of less than 10 cm. The sense of displacement in the two northern lobes (as determined by the color order in each lobe) is away from the satellite, opposite to the displacement sense in the southern lobe.

Postseismic deformation may be estimated in two ways. First, by comparing a coseismic interferogram that spans the earthquake + 1 week (Baer et al., 1999) with that of the earthquake + 3 years (Fig. 3). On the regional scale, there is no apparent difference between the two interferograms in most of the area. In more detail, however, two additional fringes are seen in the 3-year interferogram (Fig. 4b) compared to the 1-week interferogram (Fig. 4a) in the high-strained northwestern lobe. This difference may be attributed to post-

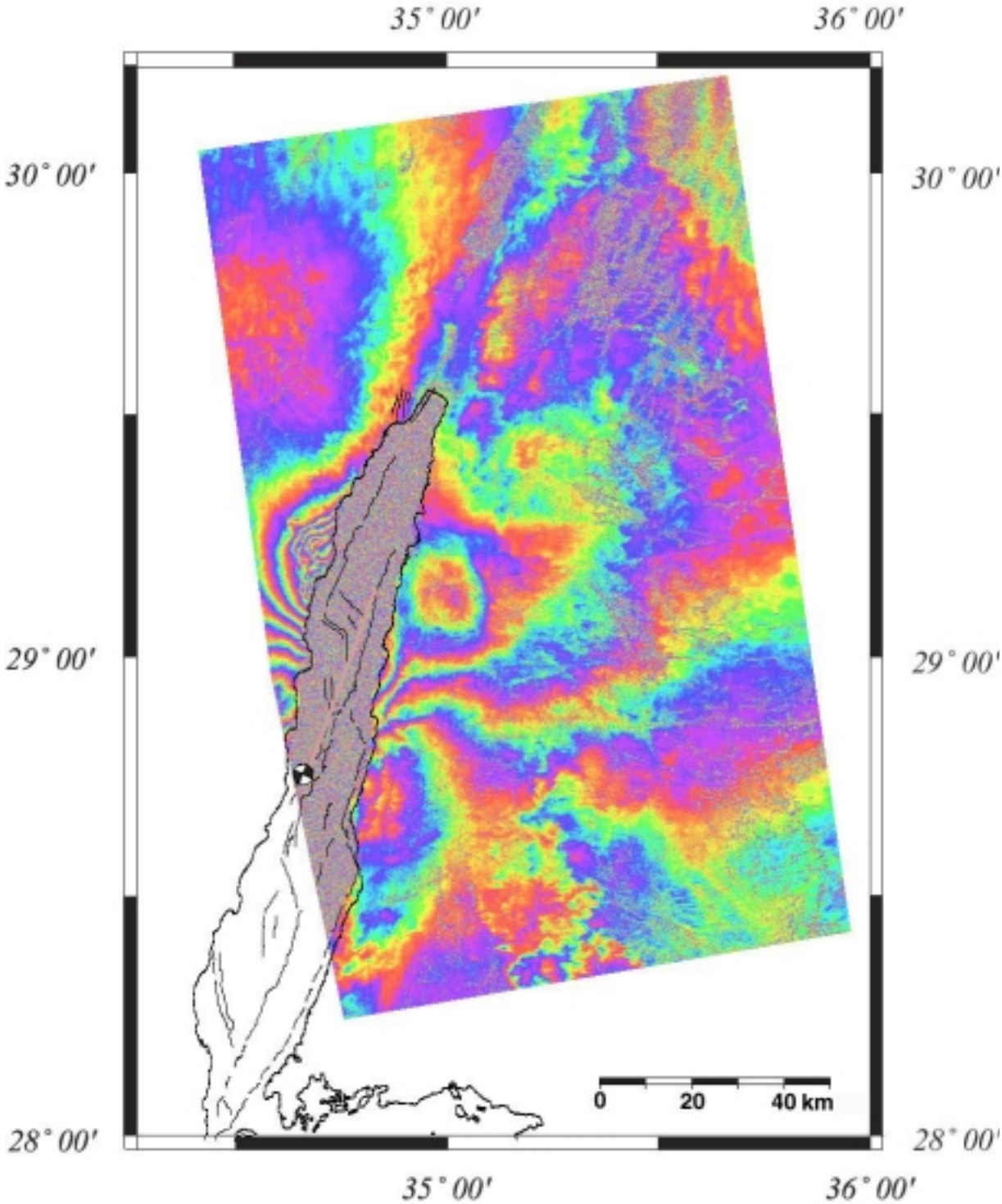

Fig. 3. Coseismic interferogram of frames 567 and 585 for the period 21/9/95–24/12/98. Each fringe cycle corresponds to 2.8 cm satellite-to-ground line of sight displacement.

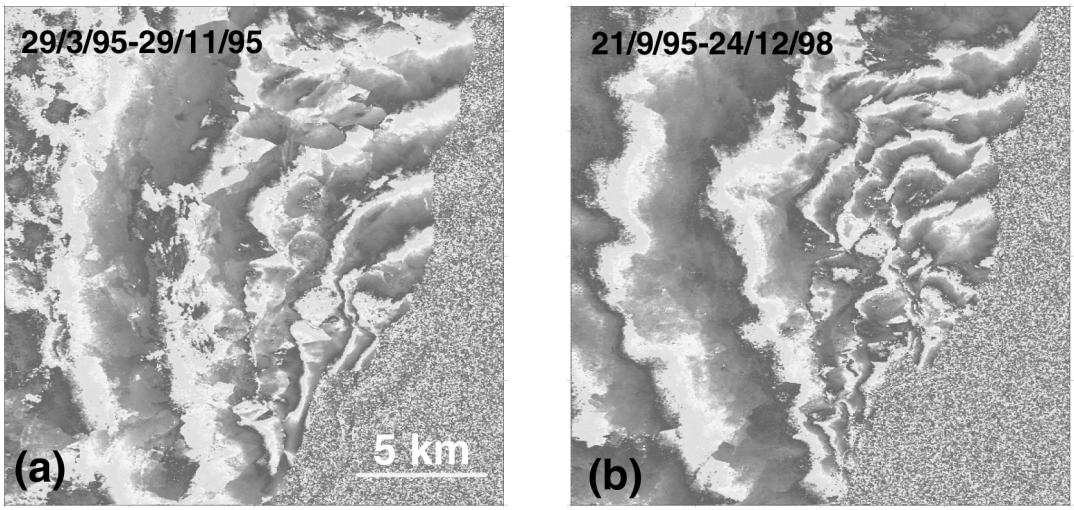

Fig. 4. Details of the area of high strain in two coseismic interferograms of frame 585. For location see Fig. 1. (a) For the period 29/3/95–29/11/95 (earthquake + 1 week). (b) For the period 21/9/95–24/12/98 (earthquake + 3 years).

seismic deformation at some time during the interval of 1 week to 3 years after the mainshock. To better constrain this deformation in time, we generated 5 postseismic interferograms of: 1 week to 6 months, 1 week to 16 months, 1 week to 38 months, 6 months to 29 months, and 18 months to 37 months after the earthquake (Fig. 5). Despite some artifacts (seen as polygonal patches), formed by errors in unwrapping the tandem interferogram used to derive the topographic phase (altitude of ambiguity for this pair is 106 m), an almost identical pattern of N–S-elongated oval fringes is seen in the first 3 interferograms (Fig. 5b–d). The sense of line-of-sight (LOS) displacement of this feature (as determined by the color order) is away from the satellite, similar to that of the coseismic displacement in this region. The amount of displacement is 2 fringes, i.e., about 6 cm, in agreement with the difference between the two coseismic interferograms shown above (Fig. 4). The pattern and spatial extent of the deformation in the postseismic interferograms are different than those in the coseismic interferograms. This local pattern of postseismic deformation is absent in the time windows later than six months after the earthquake (Fig. 5e–f), confirming that it is an early-postseismic feature which does not appear in any measurable way later on. It should be pointed out here that in the absence of post-earthquake InSAR data from the first week following the mainshock, the deformation during that week, which may comprise a significant fraction of the pure postseismic deformation, cannot be resolved separately from the coseismic deformation. Thus, the term "postseismic" used here refers to the period starting one week after the mainshock.

A six-year time-series west of the Gulf

Data acquisition along the descending track west of the Gulf (frame 3015) dates back to January 1993, and is thus considerably longer than that of the ascending track (Fig. 2). The expected horizontal displacement along the western side of the Gulf in interseismic periods is subparallel to the descending track. LOS changes reflected by interferograms made from descending track scenes are in a nearly motion-perpendicular direction and therefore reflect only a minor fraction of the total horizontal displacement. However, due to the longer acquisition history, we chose frame 3015 in order to study the longer-term deformation pattern along the Gulf. The interferograms (Fig. 6) show no detectable deformation fringes in the three years pre-earthquake interferogram or in the 6 months–37 months post-earthquake interferogram (Fig. 6a,c). Deformation fringes are observed only in time windows spanning the earthquake (Fig. 6b).

Phase gradient maps

The phase gradient was computed from the real and imaginary parts of the topography-free interferogram to highlight small-scale strain (Price and Sandwell, 1998). In the area surrounding the northern tip of the Nuweiba rupture, these maps show lineaments along

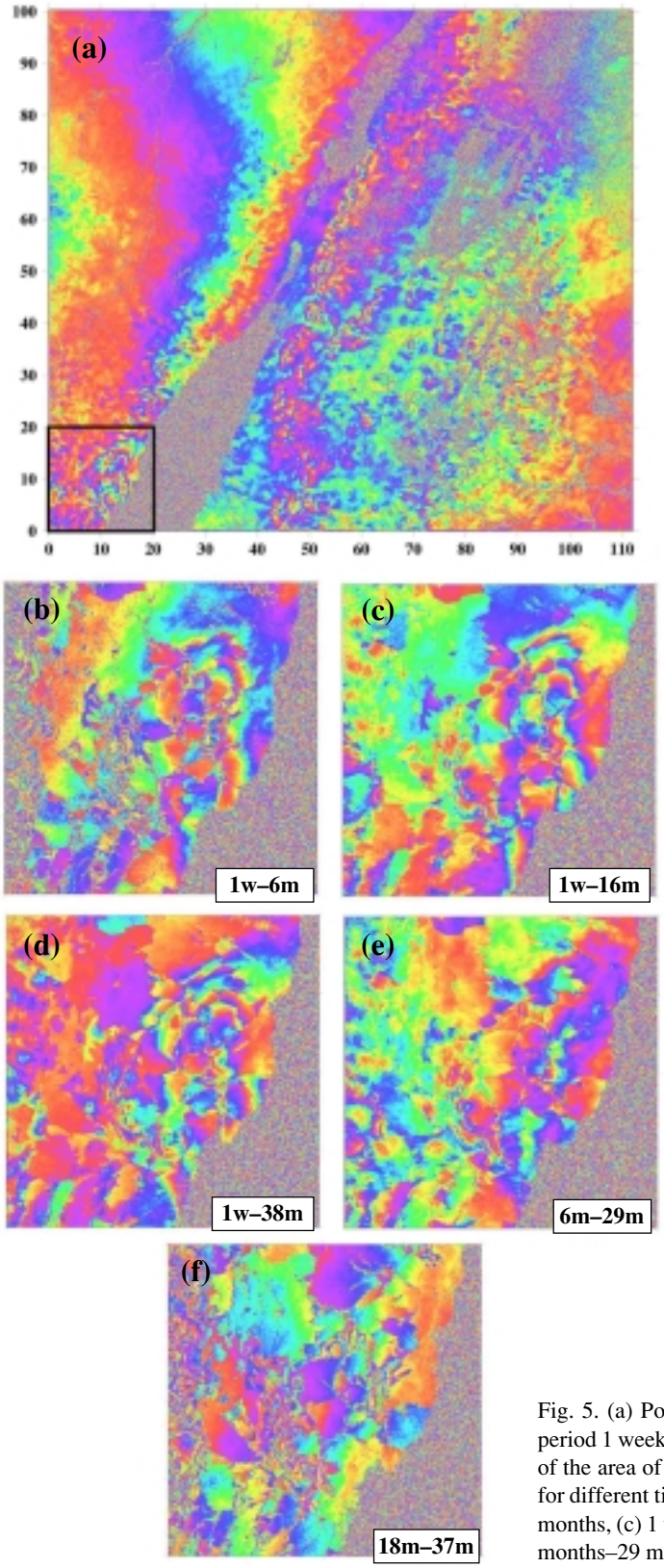

Fig. 5. (a) Postseismic interferogram of frame 585 for the period 1 week–38 months after the earthquake. (b–f) Details of the area of high strain (inset at SW corner of frame 585) for different time periods after the earthquake: (b) 1 week–6 months, (c) 1 week–16 months, (d) 1 week–38 months, (e) 6 months–29 months, (f) 18 months–37 months.

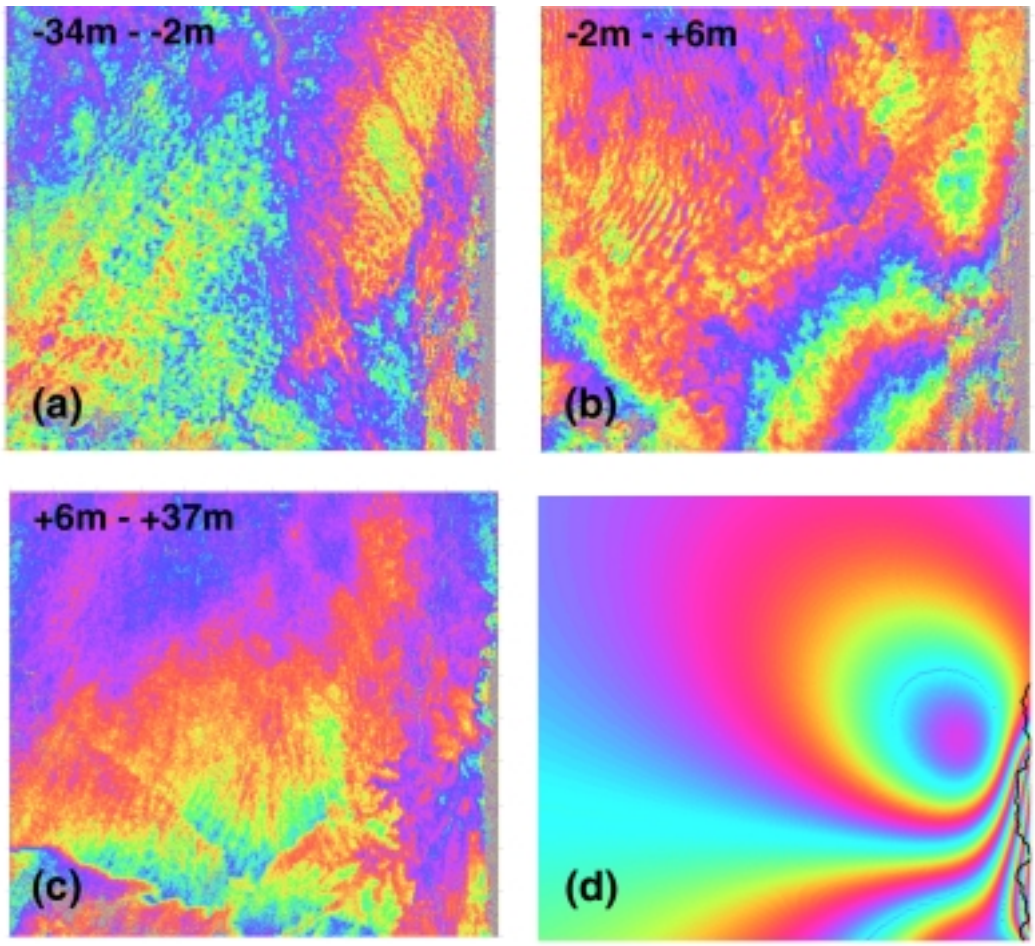

Fig. 6. Time-series interferograms in frame 3015. Width of each image is about 100 km. (a) Pre-earthquake (34 months before–2 months before earthquake); (b) coseismic (2 months before–6 months after earthquake); (c) late postseismic (6 months after–37 months after earthquake); (d) simulated coseismic interferogram (see discussion for model parameters).

both sides of the Gulf (Fig. 7). The lineaments observed on the western Gulf shore consist of single positive (dark) gradients, ramping away from the satellite (Fig. 7a). They may be interpreted either as sinistral strike-slip faults (subparallel to the main rupture) or as dip-slip faults with the Gulf side down. Range changes across these lineaments are of the order of almost a fringe cycle, namely 3 cm (Fig. 7d). The lineaments observed on the eastern Gulf shore (Fig. 7b) trend at about 30° to the main rupture trace. Each lineament consists of a positive/negative gradient pair, seen as dark/bright bands, respectively (Fig. 7b). The positive–negative couples are likely to express either extensional (open) cracks or ground subsidence above narrow graben-type faults. Each lineament expresses range changes of about half a fringe cycle (Fig. 7d), namely, about 1.5 cm.

DISCUSSION

Rupture mechanism and triggered slip during the coseismic phase

To interpret the coseismic interferograms in terms of mechanisms and absolute displacements, they were compared to simulated interferograms generated by elastic dislocation models (Okada, 1985; Feigl and Dupre, 1999). Baer et al. (1999) showed that while the location, strike, and length of the main (coseismic) rupture were well-constrained by the model interferograms, the depth of the rupture and the slip along it were not uniquely constrained. When a simple uniform dislocation model was used, the analysis showed that if the rupture reached the Gulf-bottom surface, the mean sinistral slip along the fault is constrained to about 1.4 m. If surface rupture did not occur, the

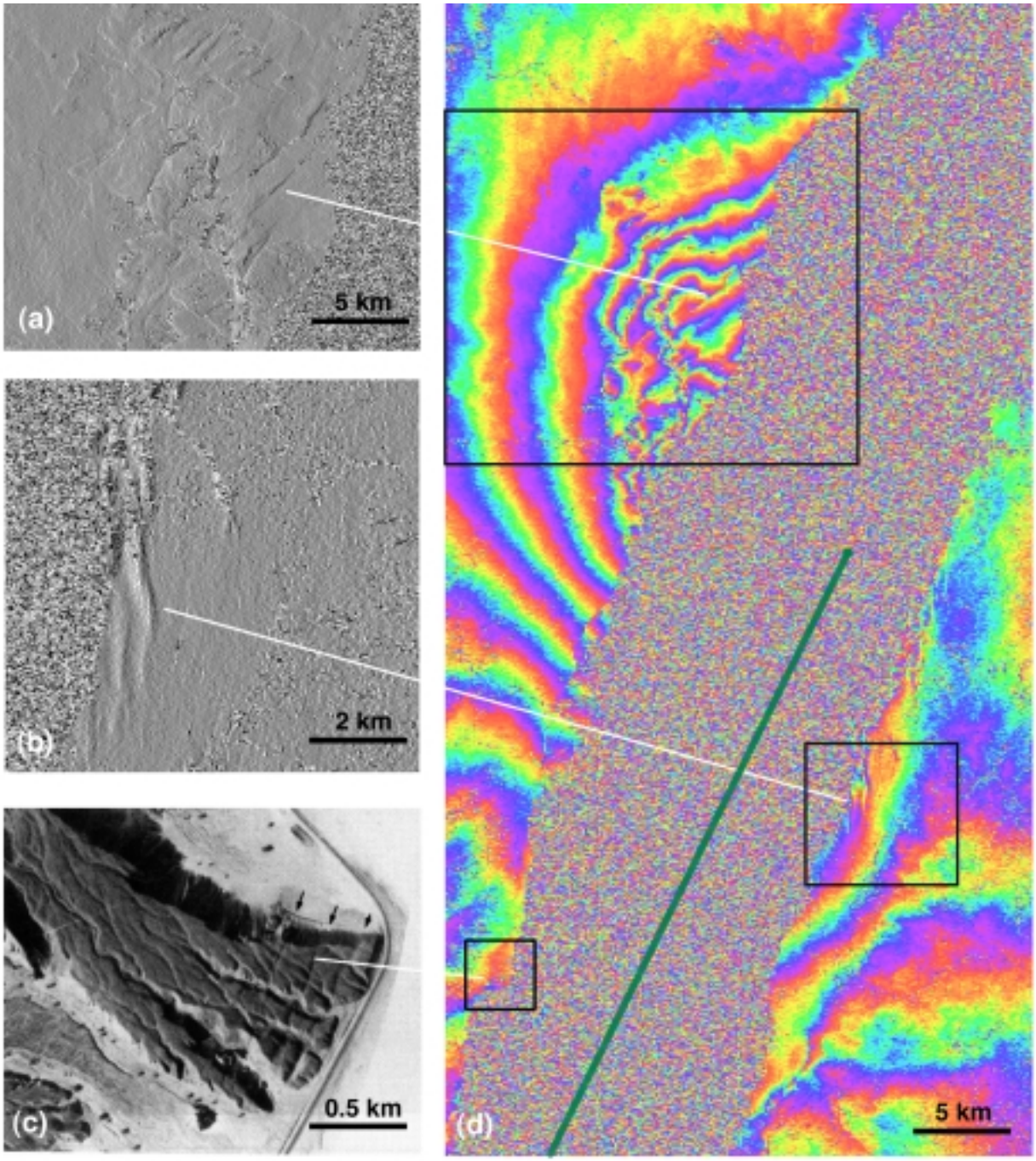

Fig. 7. Coseismic phase gradient maps showing (a) NNE-striking faults along the western shoreline of the Gulf; (b) NNW-striking extensional lineaments along the eastern shore of the Gulf. (c) Air photograph showing step fault scarps in recent alluvial fans, Wadi Huwet, eastern Sinai (from Bowman and Gerson, 1986). (d) Details of the Gulf region in the 3-year coseismic interferogram (Fig. 3). Green line marks the northern end of the earthquake rupture (see Fig. 1 for location). Note the phase discontinuities that correspond to the lineaments in the phase gradient maps (a,b) and the Gulf-parallel phase discontinuity along the western shoreline that is found at the northward continuation of the fault scarps shown in (c).

average sinistral slip could be as high as 3 m for a fault patch buried 4 km below the Gulf bottom. Different combinations of slip and burial depth could yield simulated interferograms showing good agreement with the coseismic interferogram (Baer et al., 1999). Independent evidence for the burial depth (or for Gulf-bottom surface rupturing) is currently not available.

Two examples of such coseismic simulated interferograms are shown in Figs. 6d and 8, for the descending and ascending tracks, respectively. A uniform slip of 2 m has been applied along the entire rupture, with burial depth of 1.5 km below the Gulf bottom. Both interferograms show good agreement with the coseismic interferograms (Figs. 3,6,8). A more detailed and rigorous modeling of the coseismic deformation, is currently in progress (Shamir et al., in preparation).

The lineaments described above (Fig. 7) are found only in the coseismic phase gradient maps, suggesting that they express coseismic deformation. Price and Sandwell (1998) and Sandwell et al. (2000) have shown lineaments of similar appearance in phase gradient maps of the Landers and Hector Mine earthquakes in southern California, parallel to the main

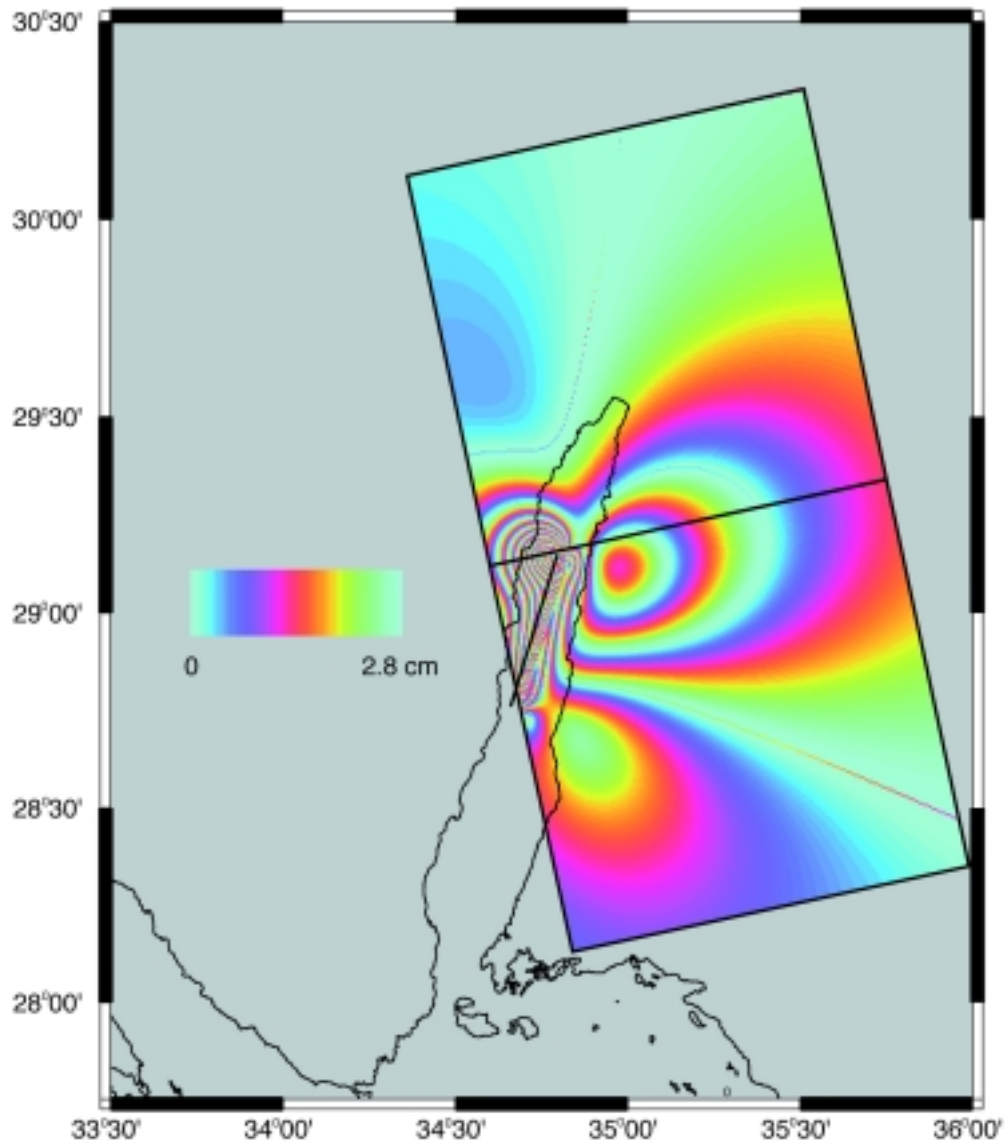

Fig. 8. Simulated interferogram showing fringes calculated from a dislocation model with one fault patch 45 km long, buried 1.5 km below sea level, with a uniform slip of 2 m. Note the good agreement with the coseismic interferogram (Fig. 3).

rupture, and related them to triggered slip on pre-existing faults. The phase gradient maps shown here may also suggest that the Nuweiba earthquake has triggered slip on secondary faults parallel to and at angles of 30° to the main rupture (Fig. 7). Fresh faults were observed immediately after the earthquake along the western shores of the Gulf (Wust, 1997; Fig. 9). Faults of similar orientations offset the Plio-Pleistocene Garof Conglomerate along the Gulf and the western margins of the southern Arava Valley (Garfunkel, 1970), and Late-Quaternary alluvial fans along the Gulf shorelines (Bowman and Gerson, 1986; Fig. 7c). Collectively, these faults suggest a long history of similar earthquakes in the Gulf and may express one of the causes of Gulf subsidence since the Pliocene.

Postseismic deformation

Various mechanisms were proposed for postseismic deformation and strain relaxation following previous earthquakes. In general, they include viscous relaxation processes at depth, slip on the original rupture or on its downward extension, and fault-zone processes such as collapse or fluid pressure buildup (e.g., Thatcher, 1983; Savage et al., 1994; Massonnet et al., 1996; Peltzer et al., 1996; Bock et al., 1997; Savage and Svarc, 1997; Reilinger et al., 2000).

We suggest that the postseismic deformation following the Nuweiba earthquake may be associated with the aftershock sequence during the first 6 months after the earthquake (Fig. 10). Almost 200 aftershocks in the magnitude range of $4.0 < M_L < 5.6$ were recorded by the Israel Seismic Network (ISN) during this period. For 58 aftershocks, regional broadband seismograms were used by Hofstetter et al. (1998) to obtain the seismic moment and the source mechanisms. In the area of postseismic deformation NW of the main rupture, several $M_L > 4$ aftershocks with normal fault mechanisms are aligned in a N–S orientation (Fig. 10). Shamir et al. (in preparation) show a good agreement

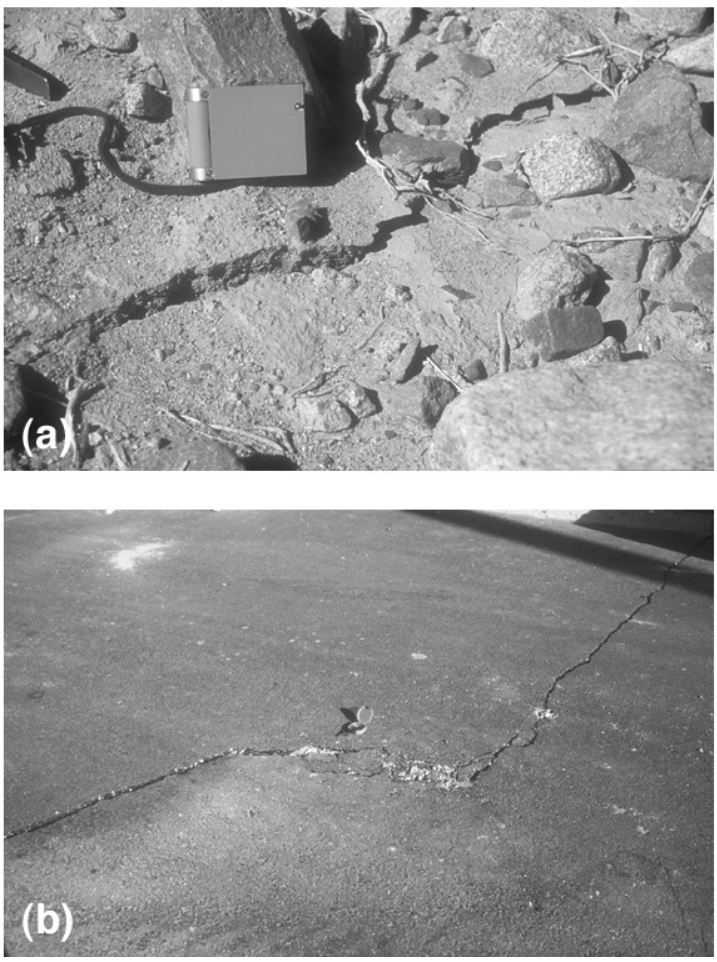

Fig. 9. Small faults observed along the Gulf of Elat immediately after the Nuweiba earthquake. (a) 2-cm vertical offset in an alluvial fan south of Nuweiba. (b) Sinistral slip indicated by transpression between two right-stepping segments of a fault across the main road north of Nuweiba.

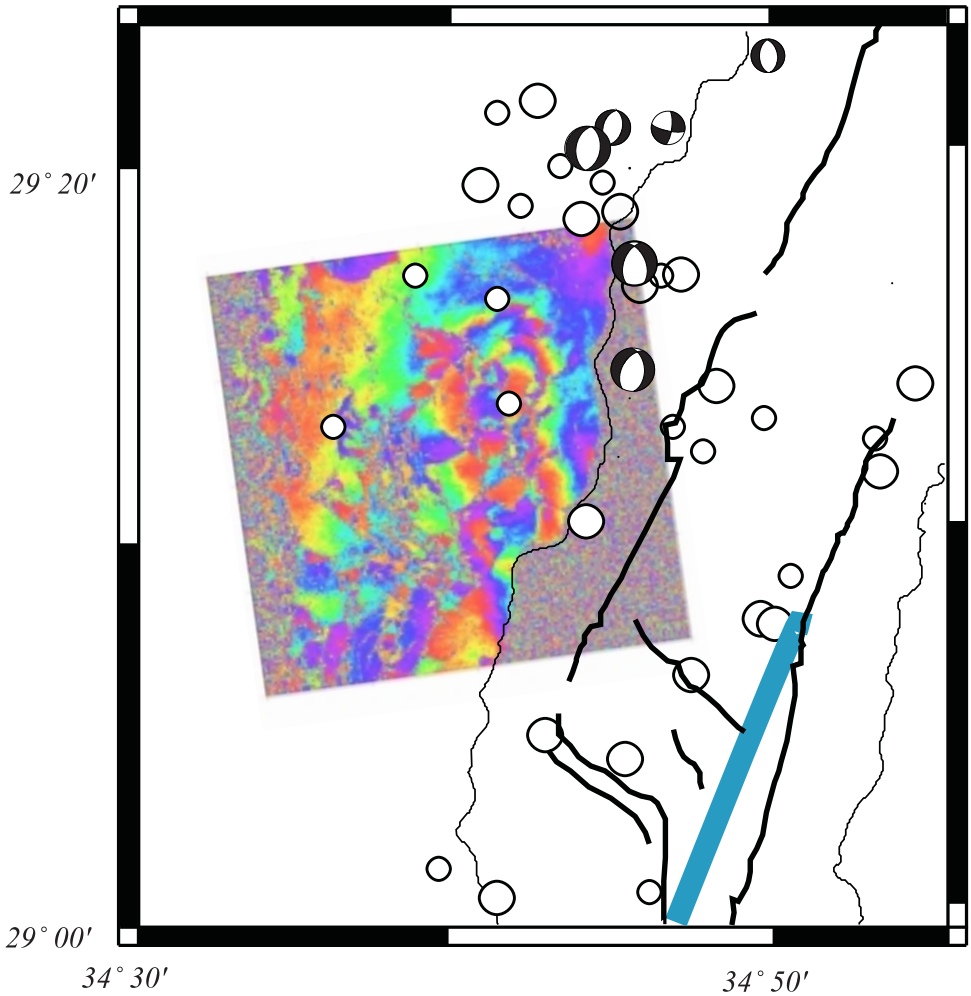

Fig. 10. Aftershocks in the range of $4.0 < M_L < 5.6$ during the first 6 months after the mainshock shown with the 1 week–6 months postseismic interferogram. The blue line marks the northern end of the earthquake rupture (see Fig. 1 for location).

between the observed deformation and model interferograms of the postseismic stage with a normal fault that coincides with the location of this aftershock sequence.

SUMMARY AND CONCLUSIONS

We used InSAR to analyze the surface deformation patterns in the region surrounding the November 1995 Nuweiba earthquake rupture during six years that span the end of one seismic cycle and the beginning of the next. Three 100 × 100 km SAR frames were used to produce interferograms for time intervals preceding, including, and following the earthquake. The pre-earthquake interferograms do not show any detectable deformation. Coseismic interferograms were made for different earthquake-spanning intervals. Comparison between the period earthquake + 1 week and earthquake + three years shows slight differences in the fringe pattern around the earthquake rupture. These differences indicate postseismic deformation later than one week after the mainshock. Detailed examination of interferograms generated for various postseismic intervals indicates that postseismic deformation is in fact limited to the first 6 months after the earthquake, is concentrated in the region of the high coseismic strain observed, and is most likely related to elastic strain relaxation by aftershocks.

The Nuweiba earthquake has presumably triggered slip on secondary faults parallel to and at angles of 30° to the main rupture. Faults of similar orientations and comparable displacements are found in Plio-Pleistocene sedimentary units (Garof Conglomerate) and

late Quaternary alluvial fans along the Gulf shores. New scarps were identified immediately after the mainshock, suggesting a long history of similar earthquakes within the Gulf.

ACKNOWLEDGMENTS

This study was supported by Grant No. 98-00134 from the United States-Israel Binational Science Foundation (BSF), Jerusalem, Israel. We would like to thank Roland Bürgmann and Kurt Feigl for their thorough and constructive reviews of this paper, which improved it significantly. Simon Williams is thanked for the dislocation modeling and InSAR simulation programs. ERS data were provided by the European Space Agency (ESA), and distributed by Eurimage, Research and Demonstration category program.

REFERENCES

Ambraseys, N.N., Melville, C.P. 1989. Evidence for intraplate earthquakes in northwest Arabia. Bull. Seismol. Soc. Am. 79: 1279–1281.

Baer, G., Sandwell, D., Williams, S., Shamir, G., Bock, Y. 1999. Coseismic deformation associated with the November 1995, M_W = 7.1 Nuweiba earthquake, Gulf of Elat (Aqaba), detected by synthetic aperture radar interferometry. J. Geophys. Res. 104: 25221–25232.

Bock, Y., et al. 1997. Southern California permanent GPS geodetic array: continuous measurements of regional crustal deformation between the 1992 Landers and 1994 Northridge earthquakes. J. Geophys. Res. 102: 18013–18033.

Bowman, D., Gerson, R. 1986. Morphology of the latest Quaternary surface faulting in the Gulf of Elat region, eastern Sinai. Tectonophysics 128: 97–119.

Feigl, K.L., Dupre, E. 1999. RNGCHN: a program to calculate displacement components from dislocations in an elastic half-space with applications for modeling geodetic measurements of crustal deformation. Comput. Geosci. 25: 695–704, .

Gabriel, A.K., Goldstein, R.M. 1988. Crossed orbit interferometry: theory and experimental results from SIR-B. Int. J. Remote Sensing 9: 857–872.

Gabriel, A.K., Goldstein, R.M., Zebker, H.A. 1989. Mapping small elevation changes over large areas: differential radar interferometry. J. Geophys. Res. 94: 9183–9191.

Garfunkel, Z. 1970. The tectonics of the western margins of the southern Arava. Ph.D. thesis, Hebrew Univ., Jerusalem, 204 pp. (in Hebrew, English abstr.).

Gilbert, G.K. 1909. Earthquake forecasts. Science 29: 121–138.

Goldstein, R.M., Zebker, H.A., Werner, C.L. 1988. Satellite radar interferometry: two-dimensional phase unwrapping. Radio Sci. 23: 713–720.

Hanssen, R. 2001. Radar interferometry: data interpretation and error analysis. Ph.D. thesis, Delft Univ. of Technology, 308 pp.

Hofstetter, A., Shamir, G., Thio, H.K. 1998. The 1995 Nuweiba source complexity and its relation with the aftershock sequence. 26th General Assembly of the European Seismological Commission, 1998, Tel Aviv, p. 28 (Abstract).

Kikuchi, M. 1995. Teleseismic analysis of the Gulf of Aqaba, Egypt, earthquake of Nov. 22, 1995. YCU, Seismology Note #49,

Massonnet, D., Feigl, K. 1995. Discriminating geophysical phenomena in satellite radar interferograms. Geophys. Res. Lett. 22: 1537–1540.

Massonnet, D., Feigl, K. 1998. Radar interferometry and its application to changes in the Earth's surface. Rev. Geophys. 36: 441–500.

Massonnet, D., Thatcher, W., Vadon, H. 1996. Detection of postseismic fault-zone collapse following the Landers earthquake. Nature 382: 612–616.

Okada, Y. 1985. Surface deformation to shear and tensile faults in a half-space. Bull. Seismol. Soc. Am. 75: 1135–1154.

Peltzer, G., Rosen, P., Rogez, F., Hudnut, K. 1996. Postseismic rebound in fault step-over caused by pore fluid flow. Science 273: 1202–1204.

Pinar, A., Turkelli, N. 1997. Source inversion of the 1993 and 1995 Gulf of Aqaba earthquakes. Tectonophysics 283: 279–288.

Price, E.J., Sandwell, D.T. 1998. Small-scale deformation associated with the 1992 Landers, California earthquake mapped by synthetic aperture radar interferometry phase gradients. J. Geophys. Res. 103: 27001–27016.

Reid, H.F. 1910. The mechanics of the earthquake. In: The California earthquake of April 18, 1906. Rep. State Earthquake Invest. Comm., Vol. 2. Carnegie Inst. Publ. 87, 192 pp., Washington, D.C.

Reilinger, R.E., et al. 2000. Coseismic and postseismic fault slip for the 17 August 1999, M = 7.5 Izmit, Turkey earthquake. Science 289: 1519–1524.

Rosen, P.A., Hensley, S., Zebker, H.A., Webb, F.H., Fielding, E. 1996. Surface deformation and coherence measurements of Kilauea Volcano, Hawaii from SIR-C radar interferometry. J. Geophys. Res. 101: 23109–23125.

Sandwell, D.T., Price, E.J. 1998. Phase gradient approach to stacking interferograms. J. Geophys. Res. 103: 30183–30204.

Sandwell, D.T., Sichoix, L., Agnew, D., Bock, Y., Minster, J.B. 2000. Near real-time radar interferometry of the M_w 7.1 Hector Mine Earthquake. Geophys. Res. Lett. 27: 3101–3104.

Savage, J.C., Svarc, J.L. 1997. Postseismic deformation associated with the 1992 M_w = 7.3 Landers earthquake,

southern California. J. Geophys. Res. 102: 7565–7577.

Savage, J.C., Lisowski, M., Svarc, J.L. 1994. Postseismic deformation following the 1989 (M = 7.1) Loma Prieta, California, earthquake. J. Geophys. Res. 99: 13,757–13,765.

Scharroo, R., Visser, P. 1998. Precise orbit determination and gravity field improvement for the ERS satellites. J. Geophys. Res. 103: 8113–8127.

Shamir, G. 1996. The November 22, 1995, Nuweiba earthquake, Gulf of Elat (Aqaba): mechanical analysis. Geophys. Inst. Isr., Lod, Rep. 550/87/96 (114).

Shamir, G. 1997. Seismicity of the southern Dead Sea Transform. Annu. Mtg. Isr. Geol. Soc., Kfar Gil'adi, p. 104 (Abstract).

Shen, Z.K., Jackson, D.D., Feng, Y., Cline, M., Kim. M., Fang, P., Bock, Y. 1994. Postseismic deformation following the Landers earthquake, California, June 28, 1992. Bull. Seismol. Soc. Am. 84: 780–791.

Tarayre, H., Massonnet, D. 1996. Atmospheric propagation heterogeneities revealed by ERS-1 interferometry. Geophys. Res. Lett. 23: 989–992.

Thatcher, W. 1983. Nonlinear strain buildup and the earthquake cycle on the San Andreas fault. J. Geophys. Res. 88: 5893–5902.

Werner, C.L., Hensley, S., Goldstein, R.M., Rosen, P.A., Zebker, H. 1992. Techniques and applications of SAR interferometry for ERS-1: topographic mapping, change detection and slope measurement. Paper presented at First ERS-1 Symposium: Space at the Service of Our Environment. European Space Agency, Cannes, France.

Wust, H. 1997. The November 22, 1995 Nuweiba earthquake, Gulf of Elat (Aqaba): post-seismic analysis of failure features and seismic hazard implications. Geol. Surv. Isr. Rep. GSI/3/97, 58 pp.

Zebker, H.A., Werner, C.L., Rosen, P.A., Hensley, S. 1994. Accuracy of topographic maps derived from ERS-1 interferometric radar. IEEE Trans. Geosci. Remote Sensing 32: 823–836.

Zebker, H.A., Rosen, P.A., Hensley, S. 1997. Atmospheric effects in interferometric synthetic aperture radar surface deformation and topographic maps. J. Geophys. Res. 102: 7547–7563.